

MAGNETAR GIANT FLARES AND THEIR PRECURSORS — FLUX ROPE ERUPTIONS WITH CURRENT SHEETS

CONG YU^{1,3} AND LEI HUANG^{2,4}

Draft version August 22, 2018

ABSTRACT

We propose a catastrophic magnetospheric model for magnetar precursors and their successive giant flares. Axisymmetric models of the magnetosphere, which contain both a helically twisted flux rope and a current sheet, are established based on force-free field configurations. In this model, the helically twisted flux rope would lose its equilibrium and erupt abruptly in response to the slow and quasi-static variations at the ultra-strongly magnetized neutron star's surface. In a previous model without current sheets, only one critical point exists in the flux rope equilibrium curve. New features show up in the equilibrium curves for the flux rope when current sheets appear in the magnetosphere. The causal connection between the precursor and the giant flare, as well as the temporary re-entry of the quiescent state between the precursor and the giant flare, can be naturally explained. Magnetic energy would be released during the catastrophic state transitions. The detailed energetics of the model are also discussed. The current sheet created by the catastrophic loss of equilibrium of the flux rope provides an ideal place for magnetic reconnection. We point out the importance of magnetic reconnection for further enhancement of the energy release during eruptions.

Subject headings: stars: magnetars — stars: magnetic field — stars: neutron — instabilities — pulsars: general

1. INTRODUCTION

Two closely related types of high-energy sources — Anomalous X-ray Pulsars (AXPs) and Soft Gamma-ray Repeaters (SGRs), are well explained as magnetars, neutron stars with super-strong ($10^{14} - 10^{15}$ G) magnetic fields (Mazets et al. 1979; Duncan & Thompson 1992; Kouveliotou et al. 1998). It is commonly accepted that dissipation of the magnetic fields drives persistent and bursting emission (Mereghetti & Stella 1995; Heyl & Kulkarni 1998; Thompson et al. 2002; Gavriil et al. 2002). More rarely and unpredictably, more violent outbursts — giant flares, have been identified. Typically, a giant flare releases a total energy of $\sim 10^{44} - 10^{46}$ ergs and shows a peak luminosity over a million times the Eddington luminosity of a neutron star (Woods & Thompson 2006; Mereghetti 2008).

There exist two principal scenarios for the place where the magnetic energy is accumulated before an eruptive outburst: in the crust (Thompson & Duncan 2001) or in the magnetosphere (Lyutikov 2006). The latter possibility was put forward to interpret the short timescale of giant flare rise time, ~ 0.25 ms (Palmer et al. 2005). It has a distinguishing feature that the energy is accumulated quasi-statically in the magnetosphere prior to the eruption, on a timescale much longer than the dynamical timescale of giant flares. The stored magnetic energy is limited by the total external magnetic energy, instead of

the tensile strength of the crust (Yu 2011b). However, the origin of the catastrophic state transitions, i.e., the transitions from a quasi-static evolution (e.g. caused by flux injections and/or crust motions) to a fast dynamical evolution, still remains a question for the magnetospheric model. Recently, Yu (2012) investigated the catastrophic mechanism of the helically twisted flux rope eruption. The author showed that, with the gradual variation at magnetar surface, either flux injections or crust gradual motions, the flux rope will evolve correspondingly quasi-statically. Once the flux rope reaches a critical height, it will become dynamically unstable and erupt to produce the giant flare. The catastrophic behavior naturally answers the above question.

Precursors to giant flares have been identified. For instance, the 2004 giant flare was preceded by a 1 second long energetic outburst event. The energy from the precursor is estimated to be about 10^{42-43} ergs. After the precursor, the magnetar entered a temporary quiescent state and stayed in the quiescent state for about 140 seconds. Then it finally gave rise to the more violent flare. It is inferred that the precursor and the giant flare are causally related (Hurley et al. 2005). This precursor is hard to explain by our previous model, since the catastrophic state transition could take place only once due to the single critical point appearing in the equilibrium curve. Additional physical elements should be included.

It is conceivable that, once the flux rope loses its equilibrium, a current sheet can be generated in the magnetosphere. This type of current sheet in magnetar magnetosphere has been hypothesized by Lyutikov (2006); Gill & Heyl (2010), which provides an ideal place for magnetic reconnection. The magnetic reconnection is of vital importance to the magnetic field dissipations (Priest & Forbes 2000; Gill & Heyl 2010; McKinney & Uzdensky 2012), which plays a crucial role

¹ National Astronomical Observatories/Yunnan Astronomical Observatory, Chinese Academy of Sciences, Kunming, 650011, China; cyu@ynao.ac.cn

² Key Laboratory for Research in Galaxies and Cosmology, Shanghai Astronomical Observatory, Chinese Academy of Sciences, Shanghai, 200030, China; muduri@shao.ac.cn

³ Key Laboratory for the Structure and Evolution of Celestial Object, Chinese Academy of Sciences, Kunming, 650011, China;

⁴ Key Laboratory of Radio Astronomy, Chinese Academy of Sciences, China.

not only in magnetars, but also in rotation-driven pulsars in general, especially in the recent observed crab nebula flares (e.g. Sturrock & Aschwanden 2012). It will contribute a sizable fraction of the total magnetic energy dissipation (Lyubarsky 1996). Secondary plasmoid instability is expected to occur in the current sheet (Huang & Bhattacharjee 2012). The bursty, non-steady character of the reconnection process marked by plasmoid ejection (Yu 2011a) is likely to induce fast variabilities in the magnetospheres. Unfortunately, no solid calculations about magnetar magnetospheres with such current sheets have been performed yet due to the complexity of this mixed boundary value problem (the magnetar surface plus the current sheet).

In this Letter, we try to explain the successive appearance of precursors and giant flares with a magnetospheric model incorporating a current sheet. This Letter is structured as follows: we briefly describe in Section 2 the basic force-free field configurations which contain both a flux rope and a current sheet, as well as the equilibrium constraints. The catastrophic responses of the flux rope to the magnetar surface variations are described in Section 3. The magnetic energy release during catastrophic state transitions is estimated in Section 4. Conclusions are given in Section 5.

2. FORCE-FREE MAGNETOSPHERE WITH BOTH CURRENT SHEET AND FLUX ROPE

The magnetosphere is assumed to be in a force-free (i.e., $\mathbf{J} \times \mathbf{B} = 0$) equilibrium state (Yu 2011a). The model is essentially the same as that in Yu (2012), except that we consider an additional current sheet in the magnetosphere.

2.1. Basic Magnetic Configurations

We show the schematic diagram of our model in the left panel of Fig.1. The toroidal force-free magnetic flux rope, shown by a thick dashed circle, is suspended by force balance in the magnetosphere at the height, h , measured from the neutron star center. In the interior of the helically twisted flux rope, the force-free solution developed by Lundquist (1950) is used. A simple relation between r_0 (minor radius of the rope) and I (current carried by the rope), i.e., $r_0 = (r_{00}I_0)/I = r_{00}/J$, is valid for such flux ropes. The quantity I_0 is related to the magnetar radius r_s and a constant Ψ_0 (with magnetic flux dimension) by $I_0 = (\Psi_0 c)/r_s$. Here c stands for the speed of light. The dimensionless current $J = I/I_0$ is the current measured in unit of I_0 . The parameter r_{00} is fixed as 0.01^5 , which is the value of r_0 for $J = 1$.

The stationary axisymmetric field configurations outside the flux rope can be expressed in terms of the magnetic stream function $\Psi(r, \theta)$ as $\mathbf{B} = \nabla\Psi \times \nabla\phi$. Note that we adopt spherical polar coordinates (r, θ, ϕ) in our calculations. The Grad-Shafranov (GS) equation can be derived according to the force-free constraint. Explicitly, it reads

$$\frac{\partial^2 \Psi}{\partial r^2} + \frac{\sin \theta}{r^2} \frac{\partial}{\partial \theta} \left(\frac{1}{\sin \theta} \frac{\partial \Psi}{\partial \theta} \right) = -(r \sin \theta) \frac{4\pi}{c} J_\phi, \quad (1)$$

⁵ For convenience of numerical calculations, lengths are measured in r_s , magnetar radius. Currents are measured in I_0 and the magnetic fluxes in Ψ_0 .

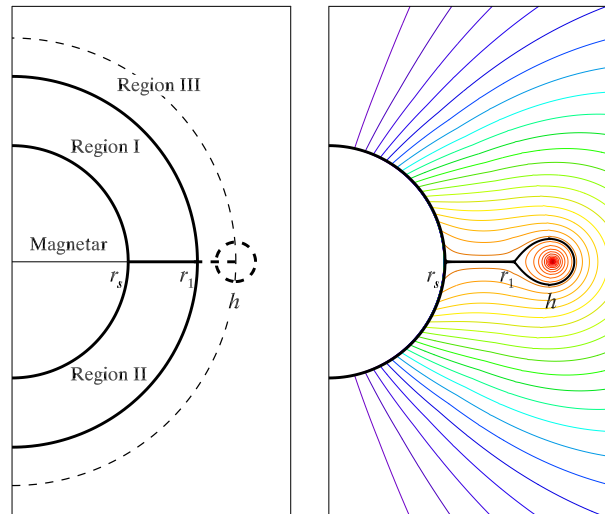


FIG. 1.— Magnetosphere containing a twisted flux rope and a current sheet. *Left*: The radius of magnetar is denoted by r_s . The current sheet is designated as the thick horizontal line at the equator, the height of which is denoted by r_1 . The twisted flux rope is designated as thick dashed circle at the equator, the height of which is denoted by h . The computation domain is divided into three regions. Solutions in different regions are obtained separately and finally melted together to form a global solution. *Right*: The magnetic field lines (thin solid line) and the current sheet (thick solid line) are shown.

where J_ϕ is the current density caused by the flux rope. We treat it as a circular ring current of the following form, $J_\phi = (I/h)\delta(\cos \theta)\delta(r-h)$ (Yu 2012). For simplicity, we use a dipolar boundary condition at the magnetar surface, i.e., $\Psi(r_s, \theta) = \Psi_0 \sigma (1 - \cos^2 \theta)$, where σ is a dimensionless quantity which dictates the magnitude of the flux at the magnetar surface.

Besides the twisted flux rope, we also include an equatorial current sheet in our model. To account for the presence of current sheet, a second boundary condition needs to be satisfied, $\Psi(r, \pi/2) = \Psi_0 \sigma$ for $r_s \leq r \leq r_1$, where r_1 denotes the tip of the current sheet. In the left panel of Fig.1, the horizontal thick solid line at the equator between r_s and r_1 represents the current sheet. Solutions to the GS equation in spherical coordinates become non-trivial due to the second boundary condition (Lin et al. 1998). Our numerical strategy is domain decomposition: the GS equation is solved in three different regions in the computational domain, labelled as region I, II, and III. The regions I and II are located between two thick solid semi-circles, $r = r_s$ and $r = r_1$, and separated by the current sheet. The flux rope lies in the region III with $r > r_1$. Solutions in the three different regions are matched together to form a global solution. An illustrative example about our basic magnetic configuration is shown in the right panel of Fig.1. Both field lines (thin solid line) and the current sheet (thick solid line) are shown. The Y-point condition, $B_\theta(r_1, \pi/2) = 0$, must be satisfied at the tip of the current $(r_1, \pi/2)$.

2.2. Equilibrium Constraints

In our catastrophic eruption model, the flux rope's dynamical behavior on short timescale is triggered by the slow and quasi-static evolution at the neutron star surface. Before the catastrophic state transition occurs, the flux rope is assumed to be in a quasi-static equilibrium. In the following, we give a brief description of the two aspects of the equilibrium constraint.

The first one is the force-balance condition, which is fulfilled if the forces exerted on the flux rope cancel each other. Simply put, the magnetic field generated by the ring current within the flux rope, $B_s = \frac{I}{ch} (\ln \frac{sh}{r_0} - 1)$ (Shafranov 1966), must be balanced by the external magnetic field B_e at $(r = h, \theta = \pi/2)$. The requirement that $B_e - B_s = 0$ can be expressed as an equation $f(\sigma, J, h) = 0$ (For details, please refer to Yu (2012)).

The second one involves the ideal frozen-flux condition, which connects the current within the flux rope and the boundary conditions at the neutron star surface. It demands that the variable $\Psi(r, \theta)$ on the edge of the flux rope $r = h - r_0$ at the equator keeps constant in the course of the flux rope's quasi-static evolution. We define another function $g(\sigma, J, h)$ to represent the value of $\Psi(h - r_0, \pi/2)$. Then the frozen-flux requirement can be explicitly expressed as $g(\sigma, J, h) = \text{const}$.

Combine the two aspects of the equilibrium constraint and we arrive at

$$\begin{cases} f(\sigma, J, h) = 0 \\ g(\sigma, J, h) = \text{const}. \end{cases} \quad (2)$$

The equilibrium curve in the following section can be obtained by solving this equation numerically (Yu 2012).

3. CATASTROPHIC RESPONSE OF FLUX ROPES TO CHANGES AT MAGNETAR SURFACE

Slowly progressing events which occur at the neutron star surface, either the crust horizontal motion (Ruderman 1991; Thompson & Duncan 2001; Jones 2003), or new magnetic fluxes continuously injected into the magnetosphere (Kluźniak & Ruderman 1998; Thompson et al. 2002; Lyutikov 2006; Götz et al. 2007), would trigger the catastrophic outburst of the flux rope. In this Letter, we focus on one aspect for brevity, i.e., the flux injections. The background magnetic field would decrease (increase) gradually, if new current-carrying magnetic fluxes of the opposite (same) polarity are injected. Two kinds of magnetic configurations in the magnetosphere, inverse and normal, are found in Yu (2012), depending on the polarity of the neutrons star's surface magnetic flux. In the normal configuration the equilibrium position of the flux rope is too close to the magnetar surface and the regular variability at the magnetar surface would contaminate the behavior of the flux rope. As a result, we will focus in this Letter on the inverse configurations.

We investigate in detail the responses of the flux rope's equilibrium height h to the changes of σ (σ reflects the background field magnitude) for the inverse magnetic configurations. Numerical results of Equation (2) are shown in a curve with thick solid segments and thin dotted segments in Fig.2. Five branches alternatively appear from bottom to top, named from I to V respectively, in the equilibrium curve according to the curve's slope in the σ - h plane. The magnetic force analysis shows

that the branches with negative slope in the σ - h diagram (h increases with decreasing σ) are stable, while the branches with positive slope are unstable (Yu 2012). There are three stable branches, I, III, and V, and two unstable branches, II and IV, in this equilibrium curve. When the surface magnetic field at the equator satisfies $B_\theta(r_s, \pi/2) = 0$, the current sheet begins to form in the magnetosphere (see blue point a^* in Fig.2). When the height of the flux rope is lower than this point, i.e., prior to the current sheet formation, the magnetic field configurations are specified in the same manner as Yu (2012). Higher than this point, the magnetic field configurations are determined according to the method outlined in Section 2. Additional unstable branches II (between points 'a' and 'b'), stable branches III (between points 'b' and 'd'), unstable branches IV (between points 'd' and 'e'), and stable branches V (higher than point 'e') show up in the equilibrium curve.

The thick solid segments in Fig.2 on the stable branches show the σ - h evolution of the flux rope. Compared to our previous work without current sheets, new features appear in the properties of the equilibrium curve. The biggest difference is that there appear two critical points, 'a' and 'd' (denoted by red dots⁶), in the equilibrium curve. As σ decreases, the flux rope moves leftward and upward along the equilibrium curve until it reaches the first critical point 'a' at $\sigma = 14.1326, h/r_s = 1.335$. The stability of the equilibrium in this system breaks after this point. During this 'loss-of-equilibrium' process σ can be regarded as unchanged because this would occur on a dynamical timescale and σ varies on a much longer quasi-static timescale. As a result, the flux rope would jump to another stable branch III with a larger equilibrium height in the equilibrium curve (see black point 'c'). On this stable branch, the flux rope can evolve on a timescale much longer than the dynamical timescale. With the further injection of magnetic flux from below, i.e., the decrease of σ , the flux rope would stay on this new stable branch for some time. When the flux rope gradually approaches the second critical point 'd' at $\sigma = 14.1298, h/r_s = 1.435$, the flux rope could not maintain its stable equilibrium and would jump to stable branch V (see black point 'f'). The two vertical jumps from critical points to another stable branches represent the catastrophic state transitions. The first state transition from 'a' to 'c' and the second one from 'd' to 'f' correspond to precursor and giant flare, respectively. The temporary quiescent state between the precursor and the giant flare corresponds to the thick solid segment on stable branch III after the first state transition. As a result, the causal connection between the precursor and the giant flare can be naturally explained by our model. When the height of the flux rope becomes larger, we find that the stable branch V asymptotically approaches a vertical line in the σ - h plane. The value of σ of this vertical line can be regarded as a threshold. If the surface magnetic flux is less than this threshold, the flux rope would reach infinity quasi-statically. Such ideal behavior occurs only when magnetic reconnection is strictly prohibited. However, this quasi-static behavior would be replaced by a

⁶ Critical points separate the stable and unstable branches of the equilibrium curve and the instability threshold lies at the critical points.

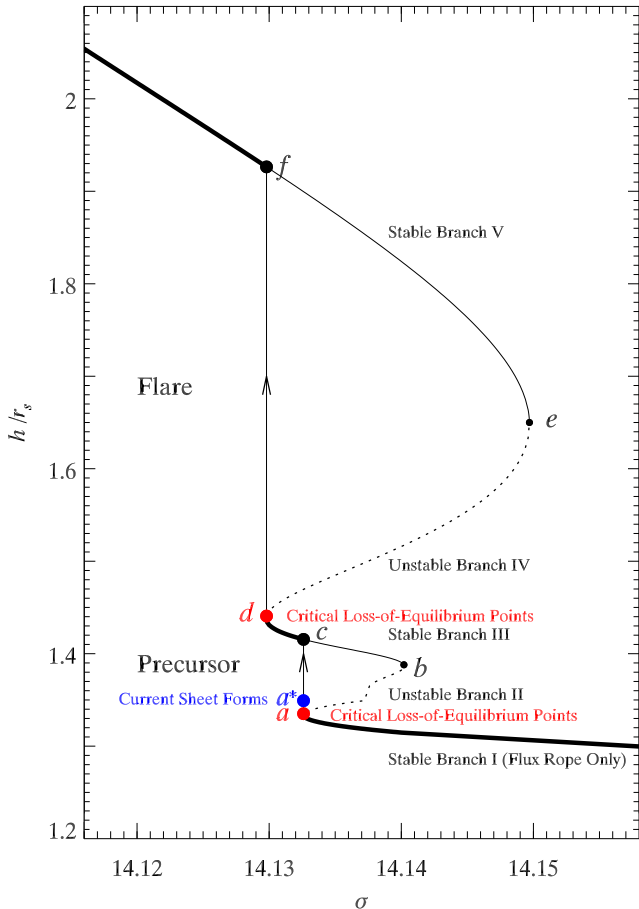


FIG. 2.— Equilibrium curve for a flux rope in magnetosphere with a current sheet. The two red dots a and d represent the critical loss-of-equilibrium points. Only the lower one a remains if the current sheet is not included. The first jump of the twisted flux rope occurs from a to c , where the flux rope reaches a lower stable branch, with the current sheet forming at the location marked with the blue point a^* . The second jump occurs from d to f , where the flux rope and current sheet reaches an upper stable branch. The two jumps are thought to correspond to the precursor and the flare, respectively.

dynamical one if magnetic reconnection proceeds sufficiently fast.

4. ENERGY RELEASE DURING CATASTROPHIC STATE TRANSITIONS

The catastrophic behavior of the flux rope also induces energy release during the state transitions. It is instructive to know the energetics of the catastrophic model. Observationally, the magnetic energy of magnetars is about $E_{\text{mag}} \sim 10^{48} (B/10^{15}\text{G})^2 (R/10\text{km})^3$ ergs. The biggest giant flare ever observed is from SGR1806-20, the energy from which is $\sim 10^{46}$ ergs. So only 1% of the magnetic energy release is already enough to explain the giant flares. A precursor with energy of $\sim 10^{42-43}$ ergs was also observed preceded this giant flare. The energy release fraction compared to the total energy is about $10^{-6} \sim 10^{-5}$.

The total magnetic energy of the magnetosphere, W_t ,

is estimated as follows,

$$W_t(h) = - \int_h^\infty F(h') dh' + W_{\text{dipole}}, \quad (3)$$

where $F = 2\pi I h (B_s - B_e)/c$ is the total force exerted on the flux rope and W_{dipole} is the magnetic energy of the background dipolar field. Note that in the above equation, we perform the work integration along the path where σ holds constant.

The energy release fraction during the ideal loss of equilibrium due to the first jump, $[W_t(h_a) - W_t(h_c)]/W_t(h_a)$ is about 4×10^{-5} (subscripts a and c correspond to points a and c in Fig.2). For a magnetar with magnetic field $B \sim 10^{15}$ Gauss, the energy release of the precursor in our model is about 4×10^{43} erg, which is already enough to explain the precursor energy release inferred from observations (Hurley et al. 2005). After the precursor, the flux rope lies on a stable branch with larger height of the equilibrium curve again. On this branch, the flux rope transits to a slow evolution stage again. This is consistent with observations that the magnetar re-enters a temporary quiescent state. With the further magnetic flux injection, the flux rope height h further increases and reach the second critical point. At this point, the second jump occurs, the energy release fraction of which, $[W_t(h_d) - W_t(h_f)]/W_t(h_d)$ (subscripts d and f correspond to points d and f in Fig.2) is higher than the first jump, approximately 0.05%. Though this value is still below the required 1% level to explain the giant flares, it is worthwhile to note that in our calculation the energy release is completely ideal. Most of the energy is locked in current sheet and we do not take into account the non-ideal effects of magnetic reconnection. When we consider the effects of magnetic reconnection, the magnetic energy lock in the current sheet would be released, and the energy release fraction can be further enhanced. This is left for a future study.

5. CONCLUSION

In this Letter we focus on the possibility of magnetospheric origin for the precursors and the successive giant flares. We put forward a force-free magnetosphere model containing a helical flux rope and a current sheet below the flux rope. The catastrophic response of the flux rope is examined in detail, taking into account the gradual process of flux injections at the ultra-strongly magnetized neutron star surface. In this model, the twisted flux rope would lose its equilibrium due to the quasi-static evolutions at the surface and finally erupt abruptly. We find that there may exist two critical points in the flux rope equilibrium curve when current sheets are taken into account. According to this new feature, the precursor and the giant flares can be naturally explained as two stages in the evolution of our models (see Section 3). The dynamical state transitions around the two critical points correspond to the precursor and the giant flares, respectively. The stable branch between the two transitions represents the quiescent state between the precursor and the giant flare.

The detailed energetics of the model are also discussed. The magnetic energy release fraction in the first jump is consistent with the precursor energy budget. The energy release fraction in the second jump, which corresponds

to the giant flare is lower than the value inferred from observations. This shows that additional energy release is necessary to account for the giant flare. The current sheet generated by the catastrophic loss of equilibrium behavior of the flux rope also provides an ideal place for magnetic reconnection, which can further enhance the energy release during the eruptions. How magnetic reconnection affects the energy release needs further investigations. Another possibility to enhance the energy release fraction depends on the boundary condition at the magnetar surface. Prior results show that dipolar boundary condition is the least efficient to release magnetic energy (Forbes et al. 1994). How do boundary conditions, such as the multipolar boundary conditions used in Yu (2012), affect the magnetic energy release is worth a further study.

The time-dependent numerical simulation of the our model is another interesting issue (Yu 2011a). Based on time-dependent models, the detailed light curves could be obtained from dynamical simulations and be com-

pared with observations. Thus certain model parameters can be further constrained by the observational light curves of giant flares.

We would like to thank the anonymous referee for instructive comments and helpful suggestions. This work has been supported by National Natural Science Foundation of China (Grants 10703012, 11173057, 11033008, 11203055, 10625314, 11121062, and 11173046), Yunnan Natural Science Foundation (Grant 2012FB187) and Western Light Young Scholar Programme of CAS and partly supported by China Ministry of Science and Technology under State Key Development Program for Basic Research (2012CB821800), the CAS/SAFEA International Partnership Program for Creative Research Teams, and the Strategic Priority Research Program on Space Science, the Chinese Academy of Sciences (Grant No. XDA04060700). Part of the computation is performed at HPC Center, Kunming Institute of Botany, CAS, China.

REFERENCES

- Duncan, R. C., & Thompson, C., 1992, *ApJL*, 392, 9
 Forbes, T. G., Priest, E. R., & Isenberg, P. A. 1994, *Sol. Phys.*, 150, 245
 Gavriil, F. P., Kaspi, V. M., Woods, P. M. 2002, *Nature*, 419, 142
 Gill, R., & Heyl, J. S. 2010, *MNRAS*, 407, 1926
 Götz, D., Mereghetti, S., & Hurley, K. 2007, *Ap&SS*, 308, 51
 Heyl, J. S., & Kulkarni, S. R. 1998, *ApJL*, 506, 61
 Huang Y. M., & Bhattacharjee A., 2012, *Phy. Rev. Lett.*, 109, 265002
 Hurley, F., et al. 2005, *Nature*, 434, 1098
 Jones, P. B. 2003, *ApJ*, 595, 342
 Kluźniak, W. & Ruderman, M., 1998, *ApJL*, 505, 113
 Kouveliotou, C., et al. 1998, *Nature*, 393, 235
 Lin, J., Forbes, T. G., Isenberg, P. A., & Démoulin, P. 1998, *ApJ*, 504, 1006
 Lundquist, S. 1950, *Ark. Fys.*, 2, 361
 Lyubarsky, Y. E. 1996, *A&A*, 311, 172
 Lyutikov, M. 2006, *MNRAS*, 367, 1602
 Mazets, E. P., et al. 1979, *Nature*, 282, 587
 McKinney, J. C. & Uzdensky, D. A. 2012, *MNRAS*, 419, 573
 Mereghetti, S. 2008, *A&AR*, 15, 225
 Mereghetti, S. & Stella, L. 1995, *ApJL*, 442, 17
 Palmer, D. M., et al. 2005, *Nature*, 434, 1107
 Priest E., & Forbes T. 2000, *Magnetic Reconnection. MHD Theory and Applications*. Cambridge Univ. Press, Cambridge
 Ruderman, M. 1991, *ApJ*, 366, 261
 Shafranov, V. D. 1966, *Rev. Plasma Phys.*, 2, 103
 Sturrock, P. & Aschwanden, M. J. 2012, *ApJL*, 751, 32
 Thompson, C., & Duncan, R. C. 2001, *ApJ*, 561, 980
 Thompson, C., Lyutikov, M., & Kulkarni, S. R. 2002, *ApJ*, 574, 332
 Woods, P. M., & Thompson, C., 2006, in *Compact Stellar X-Ray Sources*, ed. W. H. G. Lewin & van der Klis (Cambridge Univ. Press), 547
 Yu, C., 2011a, *MNRAS*, 411, 2461
 Yu, C., 2011b, *ApJ*, 738, 75
 Yu, C., 2012, *ApJ*, 757, 67